Helmholtz-Zentrum
Geesthacht
Zentrum für Material- und Küstenforschung

Original

Rogstroem, L.; Ghafoor, N.; Schroeder, J.; Schell, N.; Birch, J.; Ahlgren, M.; Oden, M.:

Thermal stability of wurtzite Zr1−xAlxN coatings studied by in situ high-energy x-ray diffraction during annealing

In: Journal of Applied Physics (2015) AIP

DOI: 10.1063/1.4927156

Thermal stability of wurtzite $Zr_{1-x}Al_xN$ coatings studied by *in situ* high-energy x-ray diffraction during annealing

L. Rogström,[1,a)] N. Ghafoor,[1] J. Schroeder,[2] N. Schell,[3] J. Birch,[2] M. Ahlgren,[4] and M. Odén[1]

[1]*Nanostructured Materials, Department of Physics, Chemistry and Biology (IFM), Linköping University, SE-581 83 Linköping, Sweden*
[2]*Thin Film Physics, Department of Physics, Chemistry and Biology (IFM), Linköping University, SE-581 83 Linköping, Sweden*
[3]*Helmholtz-Zentrum Geesthacht, Max-Planck-Str. 1, D-21502 Geesthacht, Germany*
[4]*Sandvik Coromant, SE-126 80 Stockholm, Sweden*

(Received 7 May 2015; accepted 9 July 2015; published online 21 July 2015)

We study the thermal stability of wurtzite (w) structure ZrAlN coatings by a combination of *in situ* high-energy x-ray scattering techniques during annealing and electron microscopy. Wurtzite structure $Zr_{1-x}Al_xN$ coatings with Al-contents from $x = 0.46$ to $x = 0.71$ were grown by cathodic arc evaporation. The stability of the w-ZrAlN phase depends on chemical composition where the higher Al-content coatings are more stable. The wurtzite ZrAlN phase was found to phase separate through spinodal decomposition, resulting in nanoscale compositional modulations, i.e., alternating Al-rich ZrAlN layers and Zr-rich ZrAlN layers, forming within the hexagonal lattice. The period of the compositional modulations varies between 1.7 and 2.5 nm and depends on the chemical composition of the coating where smaller periods form in the more unstable, high Zr-content coatings. In addition, Zr leaves the w-ZrAlN lattice to form cubic ZrN precipitates in the column boundaries.
© *2015 AIP Publishing LLC*. [http://dx.doi.org/10.1063/1.4927156]

I. INTRODUCTION

Transition metal (Me) aluminum nitride coatings with a cubic crystal structure generally exhibit high hardness values and may undergo high temperature age hardening due to a phase separation of the unstable cubic (c)-MeAlN phase, making them suitable for high temperature wear protection. One frequently used industrial coating is c-TiAlN, which exhibits spinodal decomposition when exposed to temperatures above 800 °C.[1] The evolving microstructure consists of nanosized c-TiN and c-AlN rich domains that result in an enhanced hardness[2,3] due to a combination of coherency strains and the elastic modulus difference between the domains.[4–6] The subsequent transformation of c-AlN to wurtzite (w)-AlN results in a loss of coherency between the binary phases and a concomitant decrease in hardness.[2,3] Recent efforts at improving the thermal stability of these coatings have focused on ways to stabilize the cubic MeAlN phase, for example, alloying[7–12] or multilayer structures.[3,13,14] ZrAlN, a related MeAlN, also exhibits good high temperature properties[15–23] and, under specific circumstances, high toughness due to a stress-induced phase transformation.[24] The ZrAlN system exhibits an even larger miscibility gap between the binary cubic phases compared to TiAlN,[25] preventing the formation of a solid solution cubic structure during growth except for low Al-contents.[16,20,25–27] ZrAlN coatings with high Al-contents form a solid solution with a hexagonal (h) crystal structure, i.e., h-ZrAlN (Ref. 20) and these coatings have shown promising cutting performance.[28] Two hexagonal ZrAlN structures, wurtzite B4 and hexagonal B_k, have been studied theoretically.[25,26] For high Al-contents, the wurtzite B4 structure is found to be the most energetically favorable, while for AlN-contents below ~68 at. %, a mixture of cubic and hexagonal B_k phases can be expected. Both hexagonal phases (B4 and B_k) are highly unstable with respect to the equilibrium binary phases (c-ZrN and h-AlN).

Studies of hexagonal structured MeAlN coatings are sparse and their high temperature behavior and thermal stability remain unexplored. For an arc evaporated h-$Zr_{0.27}Al_{0.73}N$ coating annealed for 2 h at 1000 °C, ZrN-rich layers formed within the hexagonal lattice while the mechanism behind the phase separation is not known. In that study, the coating exhibited a long-range layering due to substrate rotation during growth, thus the phase separation was likely affected by the growth conditions.[20]

In this study, we explore the thermal stability of the w-ZrAlN phase and its decomposition route in detail. The high temperature behavior of w-ZrAlN coatings grown by cathodic arc evaporation was studied using high-energy x-ray scattering techniques to follow the structure evolution *in situ* during high temperature annealing. The coatings were grown on stationary substrates to exclude the effect of artificial layering from the deposition on the decomposition route. The observed decomposition results in layered compositional modulations on the hexagonal lattice with a spatial frequency of a couple of nanometers. In addition, Zr leaves the w-ZrAlN resulting in precipitation of c-ZrN along grain boundaries.

II. EXPERIMENTAL DETAILS

$Zr_{1-x}Al_xN$ coatings were deposited using a Balzers Innova cathodic arc evaporation system. Two cathodes with

a)Author to whom correspondence should be addressed. Electronic mail: linro@ifm.liu.se

 © 2015 AIP Publishing LLC

[This article is copyrighted as indicated in the article. Reuse of AIP content is subject to the terms at: http://scitation.aip.org/termsconditions. Downloaded to] IP: 131.169.65.125 On: Mon, 27 Jul 2015 08:35:47

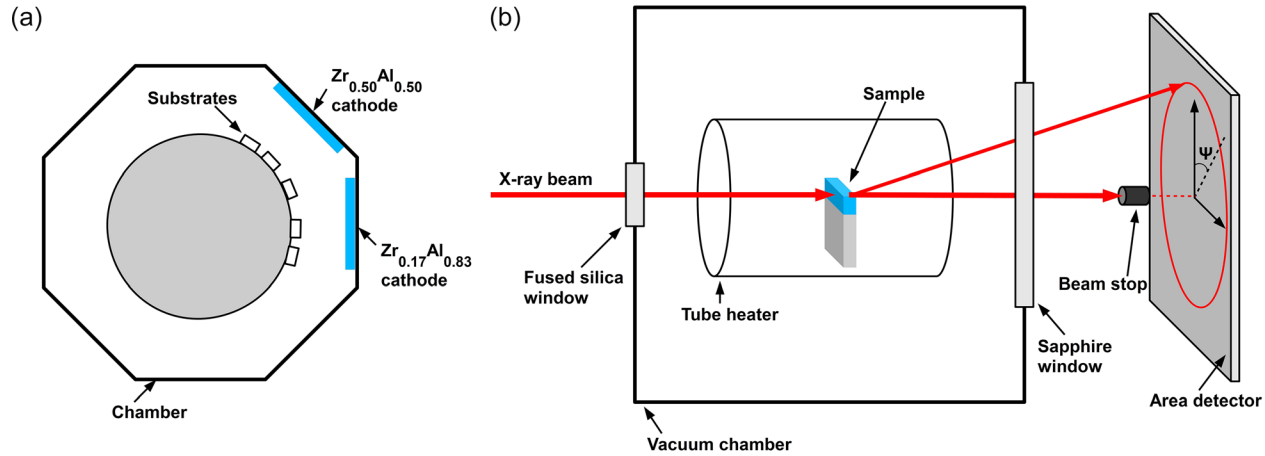

FIG. 1. (a) Top view of deposition setup and (b) the experimental setup during *in situ* x-ray scattering experiments.

Zr:Al ratios of 50:50 and 17:83 were placed next to each other in the deposition chamber (Figure 1(a)). Polished WC-Co substrates ($12 \times 12\,mm^2$) were placed at five different positions facing the two cathodes to obtain coatings with different Zr:Al ratios in the same deposition run. The substrates were kept stationary during deposition in order to simultaneously deposit different compositions and to avoid artificial layering in the as-deposited films. The deposition was performed in a mixture of Ar and N_2 (N_2:Ar flow ratio of 2:1) at a total pressure of 1.6 Pa and the deposition rate was 50–60 nm/min. The temperature during growth was 500 °C and a negative bias of 30 V was applied to the substrates.

The coating thickness was determined from fractured cross sections viewed in a scanning electron microscope (SEM, LEO Gemini). The chemical composition of the coatings was determined by energy dispersive x-ray spectroscopy (EDS) in the SEM using an Oxford X-Max detector and an electron acceleration voltage of 20 kV. The crystal structure of the as-deposited coatings was determined by x-ray diffraction (XRD) using Cu Kα radiation in θ-2θ geometry.

In situ wide and small angle x-ray scattering (WAXS and SAXS) experiments were performed during annealing at beamline P07 at PETRA III using a 78.0 keV ($\lambda = 0.158$ Å) x-ray beam. The specimens, 1 mm wide slices cut from the ZrAlN-coated substrates, were placed in a vacuum annealing chamber equipped with a resistive tube heater as shown schematically in Figure 1(b). X-ray scattering was performed in transmission geometry, whereby the x-rays were directed through the 1 mm wide sample, approximately parallel to the coating surface. The beam entered the chamber through an amorphous fused silica window and the transmitted and scattered x-ray beams exited the annealing chamber through a single crystal sapphire window. The direct beam was blocked by a 2 mm diameter beam-stop in front of the detector. X-rays scattered at wide and small angles were simultaneously collected by a 2D Perkin Elmer detector (200 μm pixel size; 2048 × 2048 pixels) placed 2700 mm downstream of the sample. The sample-to-detector distance was determined using a NIST LaB_6 standard powder. Duplicate annealing experiments (i.e., same heating procedure and exposure times) were performed on two of the samples using a shorter sample-to-detector distance (1633 mm) in order to collect more of the WAXS data. Each sample was heated at a rate of 20 °C/min to $T_{max} = 1100$ °C and held isothermally at T_{max} for 3 h before cooling down to room temperature. During heating and the isothermal stage, exposures were taken every 20th second with an exposure time of 8 s.

For more detailed analysis, the WAXS data were integrated in 10–20° wide bins in selected off-normal directions, ψ, to extract one-dimensional lineouts for different lattice planes (ψ depicted in Figure 1(b)). Pseudo-Voigt functions were fitted to the integrated 1D data to extract the plane spacing. For analysis of the SAXS data, background subtraction was performed and 1D lineouts were integrated in 20° wide bins. The layer period was extracted by fitting a pseudo-Voigt function to the 1D data using the Irena macros for Igor Pro.[29]

Microstructural analysis was performed on separate coated substrates that were annealed under identical conditions as used in the *in situ* x-ray scattering experiments. The microstructure was characterized by scanning transmission electron microscopy (STEM) using a 200 kV FEI Technai G2 instrument. A cross sectional TEM sample was prepared from one of the samples used for *in situ* WAXS experiments using a focused ion beam instrument (Zeiss 1540 EsB cross beam). In addition, cross-sectional TEM samples were prepared from coatings annealed for shorter time by mechanical polishing followed by Ar ion beam milling.

III. RESULTS AND DISCUSSION

A. As-deposited coatings

$Zr_{1-x}Al_xN$ coatings were deposited across an aluminum concentration range of $0.46 \leq x \leq 0.71$, the range being determined by the cathode compositions. The slightly lower amount of Al in the coatings, as determined by EDS, compared to the content of the used cathodes is due to re-sputtering of lighter Al atoms by the heavier Zr ions.[30] Fractured cross sections studied in the SEM reveal that all coatings have a fine-grained, smooth structure, and a thickness of 6–9 μm (not shown). Figure 2 shows θ-2θ diffractograms of the as-deposited coatings for the entire range of Al concentrations studied (i.e., $0.46 \leq x \leq 0.71$). All coatings have a hexagonal crystal structure, here assigned to a wurtzite structure. We cannot conclude that $x = 0.46$ is the lowest Al-content for which a w-ZrAlN phase can exist since the

[This article is copyrighted as indicated in the article. Reuse of AIP content is subject to the terms at: http://scitation.aip.org/termsconditions. Downloaded to] IP: 131.169.65.125 On: Mon, 27 Jul 2015 08:35:47

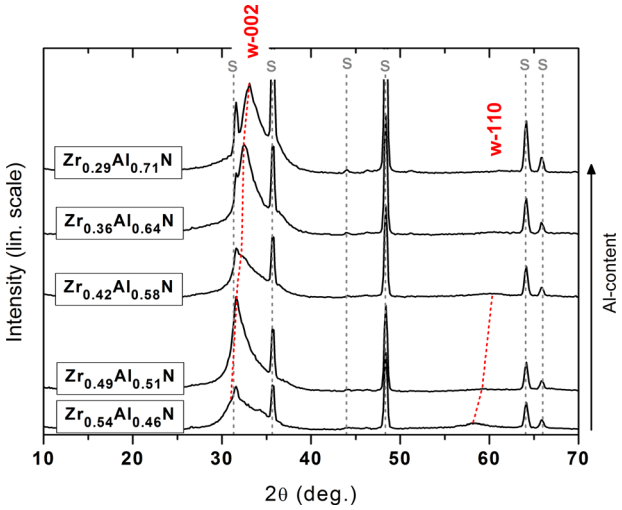

FIG. 2. X-ray diffractograms of the as-deposited coatings. The wurtzite ZrAlN 002 and 110 diffraction peaks are labeled in the figure and "S" marks the position of substrate peaks. The dashed, red line shows the approximate peak shift.

lower limit was determined by the chosen cathode composition. However, we have successfully incorporated more Zr into w-ZrAlN compared to our previous growth study[20] that used a lower deposition temperature (200 °C) and our present results agree with Hasegawa *et al.*,[31] who also used a high deposition temperature (600 °C). The higher deposition temperature results in larger ad-atom mobility during growth, which enables a higher degree of crystallization compared to the nanocomposite structure obtained in Ref. 20.

The coatings are textured with the 002 orientation close to the surface normal. The 002 texture was confirmed by WAXS for three of the samples (see below). Both the w-002 and w-110 diffraction peaks shift to larger angles with increasing Al-content, which is consistent with a decreasing lattice parameter. The shift is indicated by the red line in Figure 2 while the lattice parameters were extracted from WAXS data as discussed below. A clear w-110 peak in the lowest Al-content coating ($Zr_{0.54}Al_{0.46}N$) suggests a less strong texture for this coating, while the intensity of this peak weakens with increasing Al content.

Three $Zr_{1-x}Al_xN$ coatings (x = 0.51, 0.64, and 0.71) were selected for *in situ* x-ray scattering experiments during annealing based on the coating's chemical composition and thickness (to ensure enough diffraction signal). The x = 0.46 sample was not selected due to the lower thickness of this coating (6 μm). Figure 3 shows one-dimensional lineouts of the three as-deposited coatings, integrated in three different ψ directions to show the 002, 100, 101, and 110 diffraction peaks from the w-ZrAlN phase. The 002 signal is only observed close to the growth direction, while the 100 signal is only observed close to the in-plane direction, confirming the 002 texture. The lack of signal at smaller d-spacing values for the x = 0.71 coating is due to the different placements of the detector (see Section II). The ψ-bin positions and sizes were chosen to optimize the integrated intensity of selected peaks. The angles between the planes match well with those of a hexagonal structure. The presence of diffraction signals from different crystallographic directions suggests that the grains are rotated around the [002] axis, i.e., the c-axis. In the $Zr_{0.36}Al_{0.64}N$ coating, an additional diffraction signal is

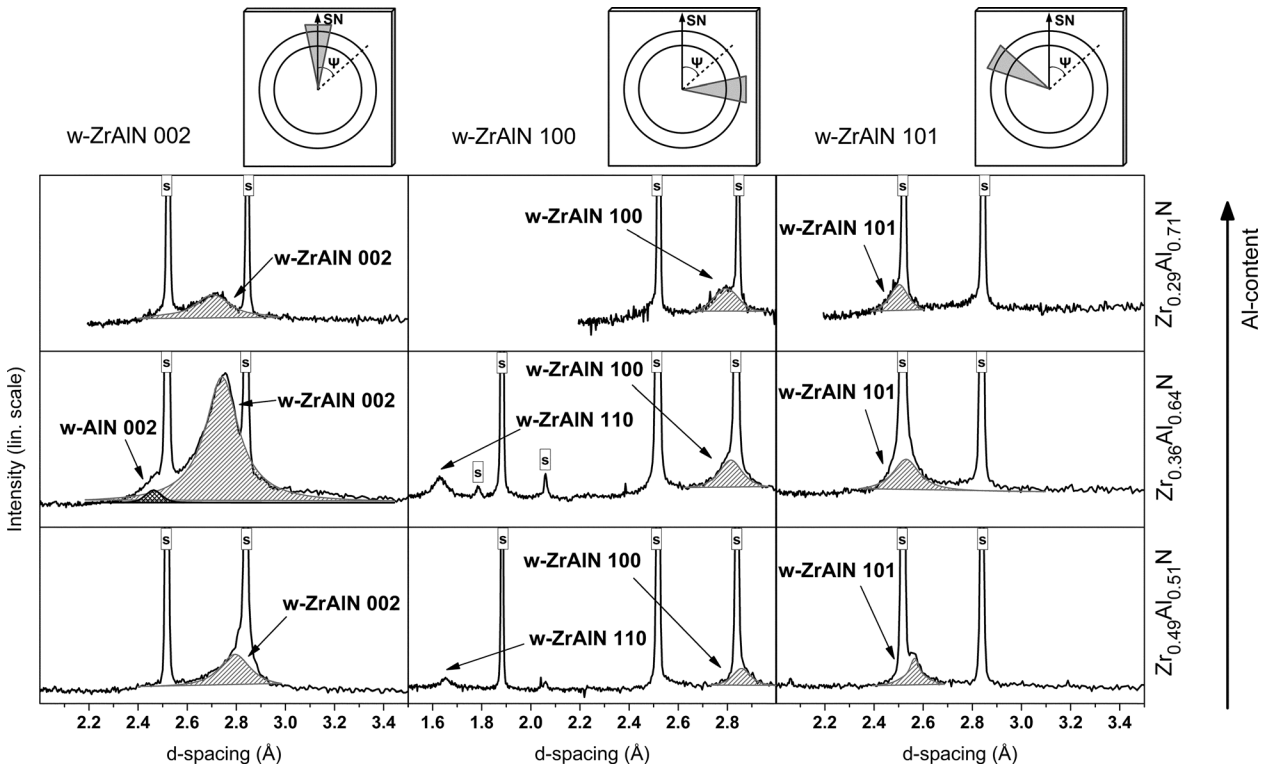

FIG. 3. Lineouts from the as-deposited coatings showing the wurtzite 002, 100, 110, and 101 diffraction peaks. "s" marks peaks originating from the substrate. The lineouts were integrated in bins centered at different off-normal angles ψ compared to the surface normal (SN) as schematically shown.

[This article is copyrighted as indicated in the article. Reuse of AIP content is subject to the terms at: http://scitation.aip.org/termsconditions. Downloaded to] IP: 131.169.65.125 On: Mon, 27 Jul 2015 08:35:47

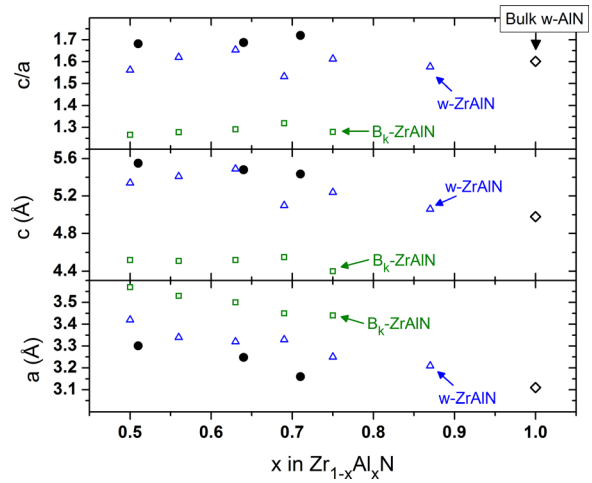

FIG. 4. Lattice parameters and c/a ratio of the as-deposited coatings (filled symbols). Open symbols shows the calculated values for the w-ZrAlN and B_k-ZrAlN structure[25] and the bulk reference value for w-AlN.[32]

observed in the same direction as that of w-ZrAlN [002] that may be assigned to w-AlN 002. The signal from this phase is weak in comparison to w-ZrAlN. Although the w-AlN 002 diffraction signal is only observed in the $Zr_{0.36}Al_{0.64}N$ sample, the detection limits of the present setup do not rule out the possibility of small amounts of w-AlN in the other samples.

Figure 4 shows the a and c lattice parameters extracted from the 002 and 100 diffraction peaks, respectively. Both lattice parameters decrease with the addition of aluminum, and for all samples, a and c are larger compared to the reference value for bulk w-AlN. Holec *et al*. calculated the lattice parameters for both wurtzite B4- and hexagonal B_k-structured ZrAlN and the values are shown in Figure 4.[25] The a and c parameters and the c/a ratio determined for the ZrAlN coatings within this work are closer to those calculated for the wurtzite B4 structure thus suggesting that the ZrAlN phase is a wurtzite structure. The c parameter is slightly larger and the a parameter is slightly smaller than the predicted values, which is likely due to a compressive in-plane stress in the arc evaporated coatings. The lattice parameters are also likely affected by the presence of point defects, such as interstitials and vacancies. Our present results show that the w-ZrAlN phase can be stabilized for Al-contents as low as $x = 0.46$, in contradiction to the prediction by Holec who found the cubic and the hexagonal B_k structures to be approximately equally stable and more stable than the wurtzite phase between $x = 0.45$ and $x = 0.68$.[25] Sheng *et al*. considered only the fcc and the wurtzite structures and found the transition point to occur at $x = 0.53$,[26] which is in closer agreement with the experimental results presented here.

Figure 5 shows parts of transformed circle sectors of the two-dimensional diffraction patterns obtained from the $Zr_{0.49}Al_{0.51}N$ coating in the as-deposited and 3 h annealed state. The sectors were transformed into 2D intensity maps with the off-normal angle ψ on the y-axis and the d-spacing on the x-axis. In its as-deposited state, the coating is textured and the width of the w-002 peak in the ψ-direction is approximately 20°. Similar w-002 peak width values are found for all three coatings. The preferred w-ZrAlN [002] growth direction with respect to the surface normal ($\psi = 0°$) differs between the three coatings and is found at $\psi = 9°$ for $Zr_{0.49}Al_{0.51}N$, $\psi = 15°$ for $Zr_{0.36}Al_{0.64}N$, and $\psi = 0°$ for $Zr_{0.29}Al_{0.71}N$. The reason for the different preferred growth directions and the [002] direction not being parallel to the substrate normal is likely a result of the placement of the stationary substrates with respect to the cathode, i.e., the ion flux was not parallel to the substrate normal (Figure 1(a)). The substrate-cathode geometry can also explain the weaker second intensity maximum originating from w-002 lattice planes at approximately $\psi = -9°$ (Figure 5(a)), as the substrate was exposed to ion fluxes arriving from two cathodes at different angles.

B. Microstructure and phase evolution during annealing

During annealing, only small changes occur for the w-ZrAlN phase. In the two-dimensional diffraction pattern recorded at 1100 °C, shown in Figure 5(b), the shift of the diffraction signal from the substrate and coating is due to thermal expansion. After 3 h at 1100 °C, c-ZrN has formed in the coating and this phase grows with its [111] direction approximately in the direction of the substrate normal for all three coatings. The c-ZrN phase grows with approximately the same mosaicity as the wurtzite phase, i.e., the width of the cubic 111 peak in the ψ-direction is 15–20° for all three coatings.

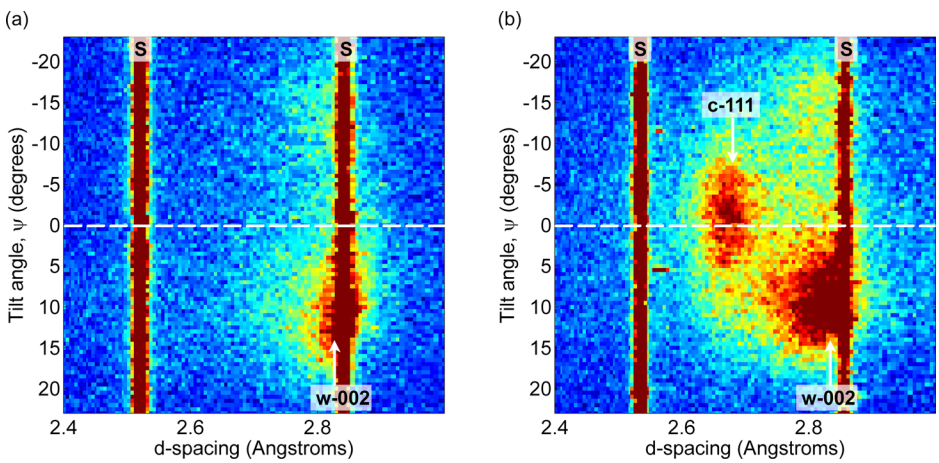

FIG. 5. Part of the two-dimensional diffraction pattern for the $Zr_{0.49}Al_{0.51}N$ coating in (a) its as-deposited state and (b) at 1100 °C, after annealing for 3 h. The dashed line marks the substrate normal direction and diffraction rings from the substrate are marked with "S."

[This article is copyrighted as indicated in the article. Reuse of AIP content is subject to the terms at: http://scitation.aip.org/termsconditions. Downloaded to] IP: 131.169.65.125 On: Mon, 27 Jul 2015 08:35:47

Figure 6(a) shows a Z-contrast STEM micrograph of the $Zr_{0.36}Al_{0.64}N$ sample after 3 h at 1100 °C (after the *in situ* WAXS/SAXS experiment). In the column boundaries, indicated by black arrows, precipitates of bright contrast are observed. These are interpreted as c-ZrN due to the absence of any other high-Zr-content phase in XRD. Within the columns, no chemical segregation is observed at this scale, thus the c-ZrN precipitates first at the grain boundaries. The diffraction contrast within the columns arises from slightly different orientations of the w-ZrAlN grains. Precipitation of ZrN at the column boundaries originates from the w-ZrAlN phase, generating an AlN-rich w-(Zr)AlN phase in the vicinity of the column boundaries. The growth of c-ZrN is slow, the size of c-ZrN grains is on the order of 10 nm after 3 h annealing at 1100 °C, suggesting limited out-diffusion of Zr from the w-ZrAlN phase. This indicates that the w-ZrAlN is relatively resistant to decomposition. Figure 6(b) shows a higher magnification STEM micrograph of the same sample as in Figure 6(a), recorded from an area within one of the columns. At this scale, compositional modulations are observed as bright and dark contrast domains, rich in Zr and Al, respectively. The compositional modulations are also observed in a sample annealed for shorter time, at 1100 °C without hold period, shown in Figure 6(c). In this case, the modulations clearly have a layered appearance with a period in the order of two nanometers. A similar period is also observed for the sample annealed for longer time (Figure 6(b)), while in this case also, larger features are observed (indicated by the arrows in Fig. 6(b)). Figure 6(d) shows a high resolution TEM micrograph of the hexagonal lattice viewed along the $[2\bar{1}\bar{1}0]$ zone axis from the sample annealed at 1100 °C without hold period. Despite chemical segregation, the crystal structure remains hexagonal. It is also possible that two crystal structures evolve that are coherent in the observed projection, but this seems unlikely since HR-imaging from different regions of this polycrystalline structure yields the same result.

Figure 7 shows lineouts for the $Zr_{0.49}Al_{0.51}N$ and $Zr_{0.36}Al_{0.64}N$ coatings as a function of time at 1100 °C. The lineouts are integrated in a ψ-bin that covers the w-ZrAlN 002 and c-ZrN 111 diffraction signals. For both coatings, the width of the w-002 diffraction peak is approximately constant with annealing time at 1100 °C although the measurement uncertainty for the $Zr_{0.36}Al_{0.64}N$ coating is rather large considering the overlap of the c-ZrN 111 peak with the w-ZrAlN 002 peak. Detailed analysis of other diffraction peaks arising from the w-ZrAlN phase (w-ZrAlN 110 and w-ZrAlN 101) also does not show any change of peak width with annealing time (not shown). The w-ZrAlN phase remains throughout the annealing process and the constant width of the w-ZrAlN diffraction peaks indicates that there is no or only limited grain growth occurring during annealing.

The amount of c-ZrN increases with annealing time, observed as an increased intensity of the c-111 peak with time, most easily observed for the $Zr_{0.49}Al_{0.51}N$ coating. In addition, a diffraction signal also appears for c-ZrN 200, most clearly in the $Zr_{0.49}Al_{0.51}N$ coating. As determined from separate lineouts (not shown) integrated in a bin selected to give the strongest c-200 signal (i.e., centered at $\psi = 55°$), the c-ZrN 200 diffraction signal first appears after 6 min at 1100 °C for $Zr_{0.49}Al_{0.51}N$ and after 30 min at 1100 °C for $Zr_{0.36}Al_{0.64}N$. The cubic 111 peak appears to sharpen in the case of $Zr_{0.49}Al_{0.51}N$, while its width is approximately constant with annealing time for $Zr_{0.36}Al_{0.64}N$. The peak sharpening is attributed to grain growth, which proceeds faster for the more unstable, higher Zr-content samples. The earlier appearance of the c-ZrN diffraction signal and the faster growth of c-ZrN grains in the higher Zr-content coating suggest that the higher Zr-content coatings are less stable, in agreement with theoretical predictions.[25,26] It should also be noted that the w-AlN peak (~2.45 Å) in the $Zr_{0.36}Al_{0.64}N$ coating does not change in intensity with annealing time, suggesting that no growth of this phase occurs. This indicates

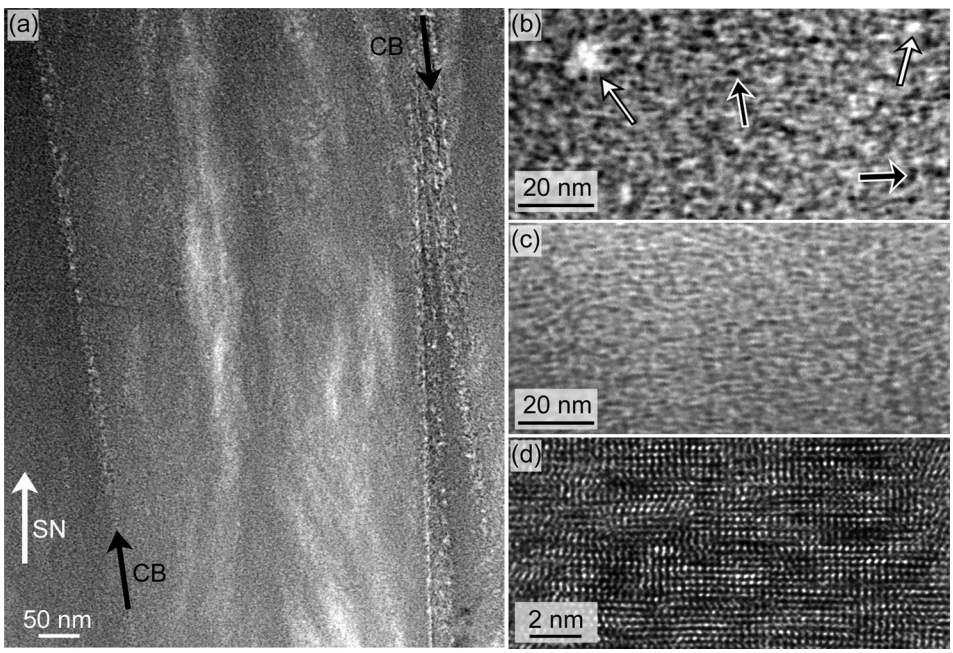

FIG. 6. Z-contrast STEM micrographs of the $Zr_{0.36}Al_{0.64}N$ coating (a) and (b) after annealing at 1100 °C with a 3 h hold; (c) after annealing at 1100 °C without hold period. (d) HR-TEM of the $Zr_{0.36}Al_{0.64}N$ coating after annealing at 1100 °C without hold period. The arrows in (a) indicate the surface normal (SN) and the location of column boundaries (CB) and the arrows in (b) point at domains enriched in ZrN (bright) and AlN (dark).

[This article is copyrighted as indicated in the article. Reuse of AIP content is subject to the terms at: http://scitation.aip.org/termsconditions. Downloaded to] IP: 131.169.65.125 On: Mon, 27 Jul 2015 08:35:47

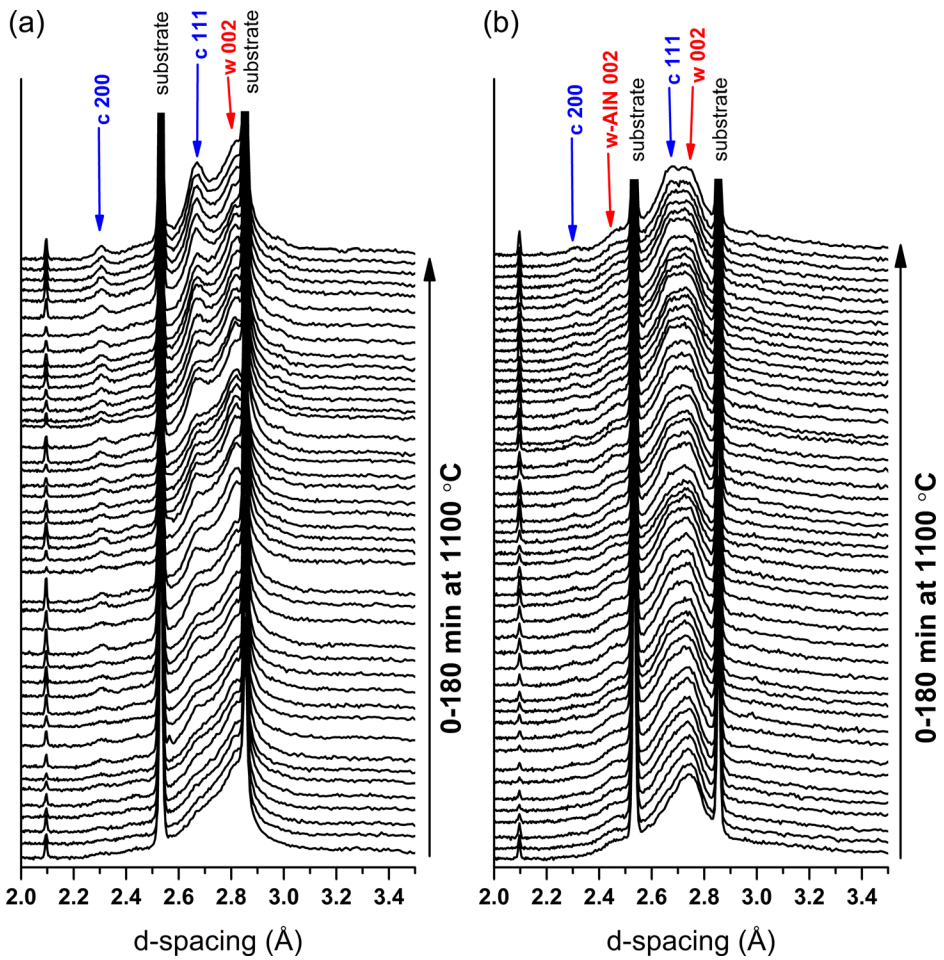

FIG. 7. Lineouts in the direction of w-002 and c-111 as a function of time at 1100 °C for (a) $Zr_{0.49}Al_{0.51}N$ and (b) $Zr_{0.36}Al_{0.64}N$. The time interval between each lineout is approximately 3.5 min.

that the decomposition of w-ZrAlN proceeds by out-diffusion of Zr to form c-ZrN, while there is no out-diffusion of Al from the w-ZrAlN phase.

The a and c lattice parameters of the w-ZrAlN phase are shown in Figure 8 as a function of ramp temperature, isothermal annealing time at 1100 °C, and composition. Only the lattice parameters from $Zr_{0.49}Al_{0.51}N$ and $Zr_{0.36}Al_{0.64}N$ are shown since the lattice parameters from $Zr_{0.29}Al_{0.71}N$ could not be extracted due to overlap of the c-111 and w-002 diffraction peaks. During the temperature ramp, both the a and c lattice parameters increase due to thermal expansion up to 900 °C whereafter the lattice parameters decrease between 900 and 1100 °C due to the annihilation of point defects, i.e., vacancies and interstitials.[33,34] During isothermal annealing at 1100 °C, the c parameter is approximately constant with annealing time for both compositions, while the a parameter is approximately constant with time for $Zr_{0.49}Al_{0.51}N$, but decreases slightly at annealing times over 100 min for $Zr_{0.36}Al_{0.64}N$. The relatively constant a and c lattice parameters with annealing time indicate that the chemical composition of the w-ZrAlN phase does not change significantly with annealing time.

Figure 9 shows the two-dimensional small angle scattering signal at different temperatures and annealing times for the $Zr_{0.49}Al_{0.51}N$ and $Zr_{0.36}Al_{0.64}N$ coatings (images for $Zr_{0.29}Al_{0.71}N$ not shown). A SAXS signal first appears around 800 °C for $Zr_{0.49}Al_{0.51}N$, around 970 °C for $Zr_{0.36}Al_{0.64}N$, and around 1000 °C for $Zr_{0.29}Al_{0.71}N$. The SAXS signal is asymmetric where higher intensity is observed close to the sample normal direction, at the positions shown by the white arrows in Figure 9, indicating that the scattering features have a small dimension close to the wurtzite [002] direction (Fig. 7). An anisotropic morphology of the segregated domains was also observed for TiAlN by SAXS during spinodal decomposition on the cubic lattice.[36] However, the anisotropy observed here is stronger and consistent with the layered structure observed by STEM (Figures 6(b) and 6(c)).The earlier appearance of the layered structure for the higher Zr-content coatings is in agreement with the prediction that higher Zr-content ZrAlN coatings are the most unstable.[25,26] The nanoscale layering revealed by the SAXS signal can arise from both differences in chemical composition and differences in crystal structure. As the extracted layer period agrees well with the period of the compositional modulations observed by STEM (see Figs. 6(b) and 6(c)), we conclude that the observed layering corresponds to differences in chemical composition within the same crystal structure. In addition, the SAXS signal from the layered structure appears well before any diffraction signal from c-ZrN can be observed. Based on these observations, the compositional modulations appear to form within the hexagonal structure.

The layer normal of the compositional modulations is found close to the w-[002] direction for all three coatings.

[This article is copyrighted as indicated in the article. Reuse of AIP content is subject to the terms at: http://scitation.aip.org/termsconditions. Downloaded to] IP: 131.169.65.125 On: Mon, 27 Jul 2015 08:35:47

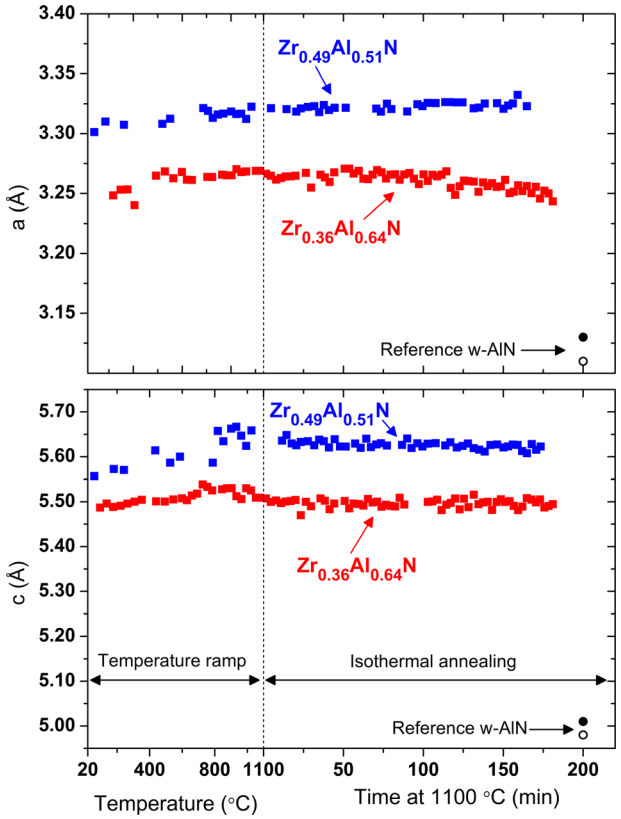

FIG. 8. The a and c lattice parameters of the w-ZrAlN phase as a function of ramp temperature and isothermal annealing time at 1100 °C. The open circle marks the room temperature value for w-AlN (Ref. 32) and the filled circle marks the value for w-AlN at 1100 °C.[32,35]

The preferential orientation of the modulations may be influenced by the overall stress state of the coating, where the stress is expected to be biaxial and thus zero in the direction of the substrate normal[37] and by the crystallographic direction. For pure w-AlN, the stiffness is similar along and perpendicular to the basal plane.[38,39] However, the elastic anisotropy of w-ZrAlN is not known wherefore this is the likely cause for the layer normal not being parallel to the surface normal.

The layer period extracted from the 2D data for all three coatings as a function of annealing time is shown in Figure 10. It is observed that once formed, the layer periods do not change with annealing time. Furthermore, the layer period depends on the Zr-content, where the smallest period (~1.7 nm) is found for the highest Zr-content coating ($Zr_{0.49}Al_{0.51}N$) and the largest period (~2.5 nm) is found for the lowest Zr-content coating ($Zr_{0.29}Al_{0.71}N$). The 2D SAXS data also reveal that there are larger features growing during annealing as observed by the increased scattered intensity at small angles, i.e., close to the beam stop. This signal arises from the c-ZrN precipitated in the grain boundaries as well as from the coarsened structure at longer annealing times (see Figure 6(b)).

No SAXS signal is observed from the as-deposited w-ZrAlN samples (not shown), suggesting a homogeneous elemental distribution in the as-deposited samples. The lack of a SAXS signal does not rule out the possibility of composition fluctuations in the as-deposited sample as random

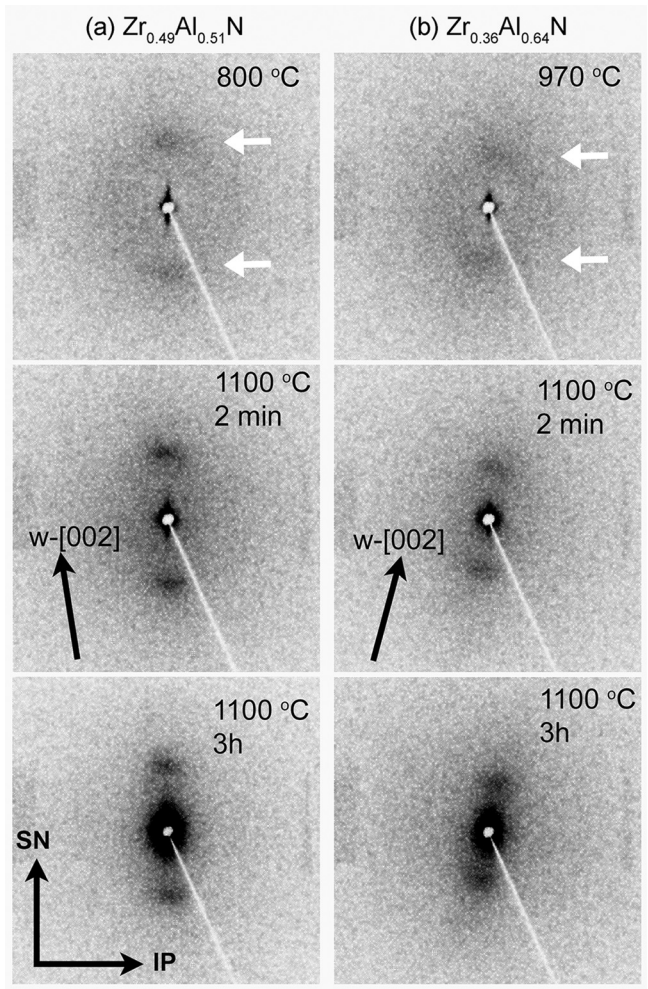

FIG. 9. SAXS signal at different annealing temperatures and times for (a) $Zr_{0.49}Al_{0.51}N$ and (b) $Zr_{0.36}Al_{0.64}N$. The white arrows indicate the position of the strongest SAXS signal. Shown is also the surface normal (SN), the in-plane direction (IP), and the w-[002] direction.

compositional fluctuations have been observed by atom probe tomography in as-deposited TiAlN coatings grown by cathodic arc evaporation,[40] while these fluctuations were too weak and disordered to be detected by SAXS using a similar

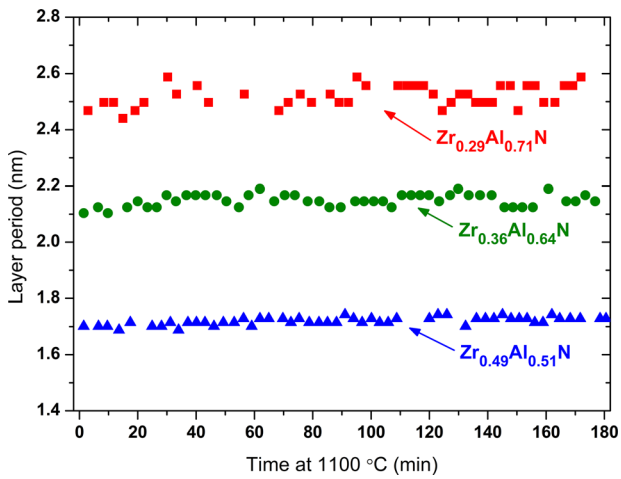

FIG. 10. Layer period extracted from the SAXS data as a function of annealing time at 1100 °C.

[This article is copyrighted as indicated in the article. Reuse of AIP content is subject to the terms at: http://scitation.aip.org/termsconditions. Downloaded to] IP: 131.169.65.125 On: Mon, 27 Jul 2015 08:35:47

experimental setup.[1] Thus, while compositional fluctuations cannot be excluded in the as-deposited w-ZrAlN samples, they are either weak or non-existent considering the stronger SAXS contrast expected between ZrN- and AlN-rich domains compared to that between TiN- and AlN-rich domains. The formation of layers during decomposition should thus not be influenced by compositional fluctuations in the as deposited sample, which was the case in a previous study.[20]

Similar compositional modulations with periods in the range of a few nm have also been observed to form in unstable wurtzite structured materials, such as w-InGaN (Refs. 41 and 42) and w-InAlGaN.[43] The layer period in w-InGaN was found to scale with chemical composition where the more unstable, high In-content coatings exhibited smaller layer periods.[42] We observe the same trend for w-ZrAlN coatings, where the size of the compositional modulations decreases with increasing Zr content. This behavior is to be expected for compositional modulations evolving during spinodal decomposition, where the wavelength of the microstructure features scales inversely with the driving force for decomposition, as was also observed for TiAlN coatings.[1] The formation of compositional modulations within the hexagonal lattice thus suggests that the mechanism for chemical segregation is spinodal decomposition. Layering due to ordering of In and Ga on the hexagonal lattice was found in InGaN coatings where both 1:1 and 3:1 ordering have been observed.[44,45] This is not the case for the w-ZrAlN as ordering of Zr and Al on the hexagonal lattice would result in additional reflections in the x-ray or electron diffraction pattern, which is not observed.

The nanoscale compositional modulations are still present after 3 h of annealing at 1100 °C and the size of the largest ZrN- or AlN-rich domains within the columns after 3 h is around 5 nm (Fig. 9(b)). The slow coarsening of the ZrN- and AlN-rich domains is in contrast to other metastable aluminum nitride systems that spinodal decompose, like c-TiAlN, where the subsequently formed w-AlN domains reach sizes of ~10 nm when ramped to 1100 °C (with no hold) under the same annealing conditions[46] or ~50 nm after annealing at 1100 °C for 2 h.[3] No stable h-ZrN phase has been observed experimentally and theoretical work suggests that a w-ZrN phase is highly unstable with respect to the fcc-ZrN phase.[26,47] Therefore, the ZrN-rich layers are expected to become unstable with increasing Zr content. The chemical composition of the ZrN-rich layers is not known and these layers might still contain a substantial amount of Al that acts to stabilize the hexagonal structure.

IV. CONCLUSIONS

Wurtzite structure $Zr_{1-x}Al_xN$ coatings with Al-contents ranging from $x = 0.46$ to $x = 0.71$ were grown by cathodic arc evaporation. The a and c parameters of the w-ZrAlN phase increase with addition of Zr. During annealing, spinodal decomposition of the wurtzite phase results in formation of nanoscale compositional modulations with a period of approximately 2 nm within the hexagonal lattice. The stability of the w-ZrAlN phase depends on chemical composition where the high Zr-content coatings are more unstable. The decomposition is initiated at temperatures of around 800 °C for $Zr_{0.49}Al_{0.51}N$, around 970 °C for $Zr_{0.36}Al_{0.64}N$, and around 1000 °C for $Zr_{0.29}Al_{0.71}N$. The period of the compositional modulations depends on chemical composition where the period is smaller for the more unstable Zr-rich coatings. In addition, out-diffusion of Zr from the w-ZrAlN phase results in nucleation of c-ZrN grains in the column boundaries.

ACKNOWLEDGMENTS

The VINN Excellence Center on Functional Nanoscale Materials (FunMat) is acknowledged for financial support. The use of PETRA III was enabled through support by the Röntgen-Ångström Cluster frame Grant No. VR 2011-6505. The authors also thank Dr. J. Zhu, Linköping University for the sample preparation by FIB.

[1]A. Knutsson, J. Ullbrand, L. Rogström, N. Norrby, L. J. S. Johnson, L. Hultman, J. Almer, M. P. Johansson Jöesaar, B. Jansson, and M. Odén, J. Appl. Phys. **113**, 213518 (2013).
[2]P. H. Mayrhofer, A. Hörling, L. Karlsson, C. Mitterer, and L. Hultman, Appl. Phys. Lett. **83**(10), 2049 (2003).
[3]A. Knutsson, M. P. Johansson, L. Karlsson, and M. Oden, J. Appl. Phys. **108**(4), 044312 (2010).
[4]L. Rogström, J. Ullbrand, J. Almer, L. Hultman, B. Jansson, and M. Odén, Thin Solid Films **520**, 5542 (2012).
[5]F. Tasnádi, I. A. Abrikosov, L. Rogström, J. Almer, M. P. Johansson, and M. Odén, Appl. Phys. Lett. **97**, 231902 (2010).
[6]R. Rachbauer, S. Massl, E. Stergar, D. Holec, D. Kiener, J. Keckes, J. Patscheider, M. Stiefel, H. Leitner, and P. H. Mayrhofer, J. Appl. Phys. **110**, 023515 (2011).
[7]H. Lind, R. Forsén, B. Alling, N. Ghafoor, F. Tasnádi, M. P. Johansson, I. A. Abrikosov, and M. Odén, Appl. Phys. Lett. **99**, 091903 (2011).
[8]L. Chen, D. Holec, Y. Du, and P. H. Mayrhofer, Thin Solid Films **519**, 5503 (2011).
[9]R. Forsén, M. P. Johansson, M. Odén, and N. Ghafoor, J. Vac. Sci. Technol. A **30**(6), 061506 (2012).
[10]R. Rachbauer, D. Holec, and P. H. Mayrhofer, Surf. Coat. Technol. **211**, 98 (2012).
[11]R. Rachbauer, A. Blutmager, D. Holec, and P. H. Mayrhofer, Surf. Coat. Technol. **206**(10), 2667 (2012).
[12]G. Abadias, I. A. Saladukhin, V. V. Uglov, S. V. Zlotski, and D. Eyidi, Surf. Coat. Technol. **237**, 187 (2013).
[13]H. C. Barshilia, M. S. Prakash, A. Jain, and K. S. Rajam, Vacuum **77**(2), 169 (2005).
[14]A. Knutsson, M. P. Johansson, P. O. Å. Persson, L. Hultman, and M. Odén, Appl. Phys. Lett. **93**, 143110 (2008).
[15]Y. Makino, M. Mori, S. Miyake, K. Saito, and K. Asami, Surf. Coat. Technol. **193**, 219 (2005).
[16]R. Lamni, R. Sanjinés, M. Parlinska-Wojtan, A. Karimi, and F. Lévy, J. Vac. Sci. Technol. A **23**(4), 593 (2005).
[17]H. Klostermann, F. Fietzke, T. Modes, and O. Zywitzki, Rev. Adv. Mater. Sci. **15**, 33 (2007).
[18]L. Rogström, L. J. S. Johnson, M. P. Johansson, M. Ahlgren, L. Hultman, and M. Odén, Scr. Mater. **62**, 739 (2010).
[19]L. Rogström, M. Ahlgren, J. Almer, L. Hultman, and M. Odén, J. Mater. Res. **27**(13), 1716 (2012).
[20]L. Rogström, M. P. Johansson, N. Ghafoor, L. Hultman, and M. Oden, J. Vac. Sci. Technol. A **30**(3), 031504 (2012).
[21]R. Franz, M. Lechthaler, C. Polzer, and C. Mitterer, Surf. Coat. Technol. **206**, 2337 (2012).
[22]N. Ghafoor, L. J. S. Johnson, D. O. Klenov, J. Demeulemeester, P. Desjardins, I. Petrov, L. Hultman, and M. Odén, APL Mater. **1**(2), 022105 (2013).
[23]P. H. Mayrhofer, D. Sonnleitner, M. Bartosik, and D. Holec, Surf. Coat. Technol. **244**, 52 (2014).
[24]K. Yalamanchili, I. C. Schramm, E. Jiménez-Piqué, L. Rogström, F. Mücklich, M. Odén, and N. Ghafoor, Acta Mater. **89**, 22 (2015).

[This article is copyrighted as indicated in the article. Reuse of AIP content is subject to the terms at: http://scitation.aip.org/termsconditions. Downloaded to] IP: 131.169.65.125 On: Mon, 27 Jul 2015 08:35:47

[25]D. Holec, R. Rachbauer, L. Chen, L. Wang, D. Luef, and P. H. Mayrhofer, Surf. Coat. Technol. **206**(7), 1698 (2011).
[26]S. H. Sheng, R. F. Zhang, and S. Veprek, Acta Mater. **56**, 968 (2008).
[27]H. Lind, R. Pilemalm, L. Rogström, F. Tasnadi, N. Ghafoor, R. Forsén, L. J. S. Johnson, M. P. Johansson-Jöesaar, M. Odén, and I. A. Abrikosov, AIP Adv. **4**(12), 127147 (2014).
[28]L. Rogström, "High temperature behavior of arc evaporated ZrAlN and TiAlN thin films," (Linköping University, Linköping, 2012), Dissertation No. 1428.
[29]J. Ilavsky and P. R. Jemian, J. Appl. Crystallogr. **42**(2), 347 (2009).
[30]A. O. Eriksson, J. Q. Zhu, N. Ghafoor, M. P. Johansson, J. Sjölén, J. Jensen, M. Odén, L. Hultman, and J. Rosén, Surf. Coat. Technol. **205**, 3923 (2011).
[31]H. Hasegawa, M. Kawate, and T. Suzuki, Surf. Coat. Technol. **200**, 2409 (2005).
[32]Joint Committee of Powder Diffraction Standards (JCPDS)—International Centre for Diffraction Data, 1998, Card No. 25-1133.
[33]P. H. Mayrhofer, F. Rovere, M. Moser, C. Strondl, and R. Tietema, Scr. Mater. **57**(3), 249 (2007).
[34]R. Forsén, M. P. Johansson, M. Odén, and N. Ghafoor, Thin Solid Films **534**, 394 (2013).
[35]G. A. Slack and S. F. Bartram, J. Appl. Phys. **46**(1), 89 (1975).
[36]M. Odén, L. Rogström, A. Knutsson, M. R. Terner, P. Hedström, J. Almer, and J. Ilavsky, Appl. Phys. Lett. **94**, 053114 (2009).
[37]D. J. Seol, S. Y. Hu, Y. L. Li, J. Shen, K. H. Oh, and L. Q. Chen, Acta Mater. **51**(17), 5173 (2003).
[38]K. Kim, W. R. L. Lambrecht, and B. Segall, Phys. Rev. B **53**(24), 16310 (1996).
[39]A. F. Wright, J. Appl. Phys. **82**(6), 2833 (1997).
[40]L. J. S. Johnson, M. Thuvander, K. Stiller, M. Odén, and L. Hultman, Thin Solid Films **520**(13), 4362 (2012).
[41]A. N. Westmeyer and S. Mahajan, Appl. Phys. Lett. **79**(17), 2710 (2001).
[42]M. Rao, D. Kim, and S. Mahajan, Appl. Phys. Lett. **85**(11), 1961 (2004).
[43]F. Y. Meng, M. Rao, N. Newman, and S. Mahajan, Acta Mater. **56**, 5552 (2008).
[44]M. K. Behbehani, E. L. Piner, S. X. Liu, N. A. El-Masry, and S. M. Bedair, Appl. Phys. Lett. **75**(15), 2202 (1999).
[45]M. Rao, N. Newman, and S. Mahajan, Scr. Mater. **56**, 33 (2007).
[46]N. Norrby, L. Rogström, M. P. Johansson-Jõesaar, N. Schell, and M. Odén, Acta Mater. **73**, 205 (2014).
[47]L. A. Salguero, L. Mancera, J. A. Rodriguez, and N. Taeuchi, Phys. Status Solidi B **243**(8), 1808 (2006).

[This article is copyrighted as indicated in the article. Reuse of AIP content is subject to the terms at: http://scitation.aip.org/termsconditions. Downloaded to] IP: 131.169.65.125 On: Mon, 27 Jul 2015 08:35:47